Journal of Water Process Engineering 55 (2023) 104064

Contents lists available at ScienceDirect

Journal of Water Process Engineering

journal homepage: www.elsevier.com/locate/jwpe

Performance evaluation of novel ml-scale microbial fuel cells using different polymeric hollow-fiber membranes

Fateme Rezaei [a], Vajihe Yousefi [a], Davod Mohebbi-Kalhori [a,b,*], Abdolreza Samimi [a]

[a] Chemical Engineering Department, Faculty of Engineering, University of Sistan and Baluchestan, Zahedan, Iran
[b] University of Sistan and Baluchestan Central Laboratory, Zahedan, Iran

ARTICLE INFO

Keywords:
Microbial fuel cell (MFC)
Hollow fiber membrane
Domestic wastewater
Electrochemical impedance spectroscopy (EIS)
Biosensor

ABSTRACT

A novel-designed milliliter-scale MFC was fabricated using three different polymeric hollow fiber membranes of Polyethersulfone (PES), Polyacrilonitryl (PAN), and Polyvinyldenfluoride (PVDF). PES, with a maximum power density of 629 mW/m^2, a current density of 1333 mA/m^2, and a coulombic efficiency (CE) of 4.22 %, achieved the best performance among the others. After that, the PAN membrane gained power and current densities of 450 mW/m^2 and 847 mA/m^2, and the PVDF membrane obtained the lowest power and current density of 63 mW/m^2 and 187 mA/m^2. For all the MFCs, the ohmic resistance incorporates only 2.5 to 5 % of internal resistance due to the small thickness of hollow fibers and the short distance between the electrodes. In the case of the PES membrane, the presence of the sulfonic group resulted in superior proton conductivity (128.10 ± 0.37 mS/cm) and reduced ohmic resistance (24.86 ± 0.07 Ω) compared to the others. Moreover, the charge transfer impedances of both electrodes for PES were nearly half of the values for PAN and about one-fifth of the values for PVDF. The increased electrical double layer capacitance nearby the electrodes of PES reveals more convenient growth of anodic *exo*-electrogenic bacteria and better accomplishment of cathodic reaction for this membrane. The COD removal efficiencies of 11.48 %, 10.55 %, and 6.48 % have been attained for PES, PAN, and PVDF, respectively.

1. Introduction

The growing concerns over fossil fuel depletion and environmental pollution issues make an urgent demand for expanding renewable energy resources [1–4]. The utilization of novel bioelectrochemical systems, including Microbial Fuel Cells (MFCs), Microbial Electrolysis Cells (MECs), and Microbial Desalination Cells (MDCs), offers the possibility of renewable energy production and addressing environmental concerns simultaneously [5–7]. Recently the MFC technology, in which the embedded chemical energy of organic and some recalcitrant inorganic compounds of waste materials convert to clean electricity, has significantly gained interest among academic researchers [3,8]. The electricity generation contemporary with pollutant remediation, and the availability of industrial and human wastes as infinite gratis row material, are some of the MFC primacies over the other bioelectrochemical or treatment methodologies [9].

MFCs generally have two chambers for the anode and cathode reactions, separated by a proton exchange membrane (PEM). In the anode chamber, protons and electrons are generated during the oxidation of substrates using electrochemically active microorganisms [10]. Then, the electrons are transferred via the external circuit, and simultaneously protons are conveyed through PEM toward the cathode electrode to accomplish the oxygen reduction reaction [11]. The MFC studies are focused not only on treatment efficiency but also on gaining high electrical power production. However, the obtained power is less than the theoretical banded chemical energy of substrates due to the irreversible overpotentials [12]. Improving the performance of MFCs is possible by optimizing process parameters such as reactor configuration [13], temperature, and medium pH, which could involve the metabolic activity of anodic biofilm [14], or by choosing proper cost-effective materials or efficient structure and design for the MFC constituents including the electrodes and PEMs [15,16]. Optimization of the MFC electrodes could be performed by focusing on the anodic current collector [17], the number of anodes [18,19], presenting state-of-the-art structure and material for anode electrode [20–23], modification of typical anode materials [19,24,25], or enhancing the performance of a cathodic section of MFCs [26], particularly by introducing innovative and economic cathodic catalysts [27,28].

* Corresponding author at: Chemical Engineering Department, Faculty of Engineering, University of Sistan and Baluchestan, Zahedan, PO Box: 98164-161, Iran.
E-mail addresses: v.yousefi@eng.usb.ac.ir (V. Yousefi), davoodmk@eng.usb.ac.ir (D. Mohebbi-Kalhori).

https://doi.org/10.1016/j.jwpe.2023.104064
Received 30 January 2023; Received in revised form 4 July 2023; Accepted 14 July 2023
Available online 1 August 2023
2214-7144/© 2023 Published by Elsevier Ltd.

However, finding the proficient PEM is the most serious bottleneck of MFC commercialization which cause underperformance and accounts for approximately 40 % of the capital cost of MFCs [15,29,30]. Although the MFC systems could operate without membranes, membrane-less MFCs suffer from several obstacles, including substrate and oxygen crossover and cathode contamination, which has limited their practicability [31]. On the other hand, insufficient proton conductivity of available PEMs resulted in pH splitting, the internal resistance elevation, and hindering the overall performance of MFCs [32].

A wide variety of membranes have been explored for MFC application which could be categorized as two general groups of non-porous and porous separators. Non-porous membranes include ion exchange membranes (IEMs) and forward and reverse osmosis (FO/RO) membranes. The IEMs are ion-selective membranes that transmit the species based on their embedded ionic functional groups, including cation exchange membranes (CEMs), anion exchange membranes (AEMs), and bipolar membranes (BPMs) [16,33]. Several CEMs have been implemented in MFC systems, such as Nafion [34,35], Hylfon [36], Zirfon [37], and CMI 7000 [29,38]. Nafion is the most well-known CEM, which has proper ion conductivity and acceptable proficiency in polymer electrolyte membrane fuel cells (PMFCs). However, the limited proton conductivity, high cost, pH imbalance, excessive oxygen and substrate permeability, and bio-fouling hinder its applicability for MFCs. Zirfon and Hylfon are more conductive and chemically stable but have a higher internal resistance than Nafion [32,37]. CEMs mostly suffer from poor proton conductivity and pH splitting [31]. Although AEMs have better pH balance and proton conductivity using phosphate or bicarbonate as a pH buffer, they are more susceptible to deformation [33,39].

On the other hand, porous membranes could transmit species based on their size and shape. Porous separators include nanofiltration (NF), micro-filtration (MF), ultrafiltration (UF), and coarse-pore membranes [40,41]. As a substitute for expensive and inefficient IEMs, several cost-effective porous separators such as composite membrane [38,42–44], J-cloth [45,46], glass fiber [45,47], nylon mesh [45], stainless steel mesh, and ceramic membranes [48–56] have been inspected to improve the MFC performance [41,57].

Even though MFC technology faces significant improvement in wastewater treatment and power production, this technique has not been capable of going beyond the lab scale owing to its complicated nature, low power output, expensive materials, and long-term instability [58,59]. Recently, ml-scale MFCs have witnessed significant upward progress due to the potential applications in powering small portable electronic devices in remote locations and biosensors [60–62]. Small-scale MFCs provide a large surface-to-volume ratio, lower ohmic resistance, convenient fabrication, and versatile designs [38,63,64]. Furthermore, they introduce a viable method for scaling up the technology by stacking multiple small MFC units [65,66].

In this respect, the highest power and current densities have ever been reported by Fan et al. (2021) using a miniature single-chamber MFC which was fabricated by an innovative composite anode made of multi-wall carbon nanotubes (CNTs) and chitosan (CHI) hydrogel. They obtained an extreme power density of 5615.7 mW/m^2 and nearly 60,000 mA/m^2 current density. The diminutive internal resistance (Rin = 82 Ω) as a result of highly conductive, hydrophile, and biocompatible anode structure, and a short distance between the electrodes, was reported as the probable reason for the excellent MFC performance [67]. After that, Ringeisen et al. (2006) used a 1.2 ml miniature cylindrical MFC equipped with Nafion 117 membrane. They obtained the maximum power and current densities of 400 mW/m^2 and 800 mA/m^2 using reticulated vitreous carbon (RVC) electrode and 4000 mW/m^2 and 11,000 mA/m^2 using a graphite felt electrode, respectively [68]. Similarly, Richter et al. (2008) reported relatively high current densities of 688 and 3147 mA/m^2 using flat gold and carbon cloth electrodes, respectively, in an ml-scale MFC working by Nafion 117 as PEM [69]. The other intensified power and current production of 1800 mW/m^2 and 6000 mA/m^2 were observed by Fan et al. (2007) in a 2.5 ml MFC using a J-cloth separator instead of common polymeric PEMs [46].

However, all the ml-scale MFC studies did not have such extreme power and current proficiency. For instance, Ieropoulos et al. (2010), who investigated a 25 ml MFC equipped with a Hylfon membrane, achieved the maximum power density of 80 mW/m^2 using the stack of four MFC units [36]. Papaharalabos et al. (2015) fabricated single chamber MFCs (5.22 ml) using three different rapid prototyping materials with CMI-7000 membrane, which were fed by human urine (1 ml/h). The overall stack output power and current density for PG-ISO (medical-grade biocompatible Polycarbonate) fabricated MFC was 3.6 mW/m^2 and 9.1 mA/m^2, respectively [38]. Furthermore, Lim et al. (2012) investigated the behavior of two chamber MFC with distinct polymeric membranes such as Nafion 117, Nafion 112, PES, and PES/SPEEK. They showed that adding SPEEK to PES increases the hydrophilicity of the PES membrane, and according to their findings, the PES membrane with 5 % SPEEK has the highest performance compared to the others with the maximum power and current densities of 6.665 mW/m^2 and 17.527 mA/m^2 [42]. Shahgladi et al. (2014) evaluated the performance of the MFC by synthesized PVDF/Nafion membrane fed by an artificial substrate. The results show that a blend of 0.4 g Nafion with PVDF had higher power density (4.9 mW/m^2) and CE (12.1 %) due to the higher conductivity. They also compared the results with neat Nafion 117 and concluded that blending PVDF with Nafion not only enhances the power output but also decreases the operational costs [44]. An overview of the electricity generation performance of ml-scale MFCs is summarized in Table 1. The miniature MFC systems, from milliliter to microliter scale, were also reviewed by Qian and Morse [63]. Moreover, the potential applicability of small MFCs, mostly microliter scale and microfluidic systems, as biosensors have attracted much attention recently [60,61,70].

In the present research, the feasibility of bioelectricity generation using three commercial hollow fiber membrane types, including Polyether sulfone (PES), Polyacrylonitrile (PAN), and Poly Vinylidene Fluoride (PVDF), have been assessed in a novel-designed milliliter scale MFC. The hollow fiber membranes have been investigated according to their cost-effectiveness, mechanical properties, and hydrophilicity. Moreover, the performance of MFCs has been evaluated in terms of maximum power output, coulombic efficiency, and COD removal efficiency. The internal resistance components have been identified by the equivalent electrical circuit (EEC) modeling over the results of the electrochemical impedance spectroscopy (EIS) analysis. To the best of the author's knowledge, there is no study to evaluate the performance of such a small-scale tubular microbial fuel cell with a polymeric hollow fiber membrane.

2. Materials and methods

2.1. MFC construction and operation

Three identical tubular MFCs were designed and constructed by drilling down two half-cylinder holes, which create a cylindrical bed (3 mm depth and 110 mm length) inside the cubic Plexiglasses. This cylinder was used as the anodic chamber with a total working volume of 3.1 ml. A single hollow fiber was inserted into the anode chamber as the proton exchange membrane, and its internal volume was used as the cathode chamber of the milliliter-scale MFCs. Three types of hollow fibers, including Polyether Sulfone (PES, 1 mm outer diameter, 0.1 mm thick, pore size of 200 nm, SPECTRUM® Laboratory), Polyacrylonitrile (PAN, the internal diameter of 0.825 mm and outer diameter of 1 mm, pore size of 30 nm, Parsian Pishro Sanat Polymer Co., Iran), and polyvinylidene fluoride (PVDF, inner diameter of 1.02 mm and outer diameter of 1.3 mm, pore size of 30 nm, Parsian Pishro Sanat Polymer Co., Iran) was implemented as PEM which were stored separately in deionized water before use.

The Anode electrode was the carbon cloth (7.2 μm fiber diameter, % 95 carbon content, Pantex®35, Zoltek Co. Ltd., USA) that was wrapped

Table 1
The overview of demonstrated ml-scale MFCs in the literature.

Anode volume (ml)	Anode (surface area)	PEM (surface area)	P_{max}(mW/m^2)	I_{max}(mA/m^2)	Ref.
1.2	RVC[a] (37 cm^2)	Nafion 117 (2 cm^2)	400	800	[68]
	GF[b] (610 cm^2)		4000	11,000	
7	Gold (7.8 cm^2)	Nafion 117 (2 cm^2)	NA[c]	688	[69]
	Carbon cloth (6.45 cm^2)		NA[c]	3147	
5.22	Carbon fiber (155 cm^2 folded 5 times)	CMI-7000 (12 cm^2)	3.6	9.1	[38]
25	Carbon fiber (270 cm^2)	Hylfon (NA[c])	80	50	[36]
6.3	Carbon fiber veil (67.5 cm^2)	PEM[j] (2.25 cm^2)	0.41	3	[71]
2.5	Carbon cloth (14 cm^2)	J-cloth (14 cm^2)	1800	6000	[46]
7.5	Carbon rod (0.5 mm diameter)	GORE-SELECT[d] (N/A)	22	850	[62]
~28.26	Carbon fiber brush (2.5 cm diameter, 2.5 cm length)	nonwoven fabric (7 cm^2)	3921	24,519	[72]
42.5	Carbon paper (15 cm^2)	PES/SPEEK[e] 3 % (2.54 cm^2)	0.065	0.181	[42]
		PES/SPEEK[e] 5 % (2.54 cm^2)	6.665	17.527	
		PES[f] (2.54 cm^2)	0.030	0.011	
		Nafion 112 (2.54 cm^2)	0.003	0.124	
		Nafion 117 (2.54 cm^2)	3.630	9.842	
100	NA[c] (12 cm^2)	PVDF[g]/Nafion(N/A)	4.9	57.6	[44]
1.5	CHI/CNT hydrogel[h] (0.196 cm^2)	No PEM (single chamber)	5615.7	~60,000	[67]
2.75	Carbon cloth (~9.5 cm^2)	PES[f] (3.42 cm^2)	629	1333	This study
		PAN[i] (3.45 cm^2)	450	847	
		PVDF[g] (4.49 cm^2)	63	187	

[a] RVC: Reticulated vitreous carbon.
[b] GF: Graphite felt.
[c] N/A: not available.
[d] GORE-SELECT: a commercial ePTFE-reinforced composite membrane.
[e] SPEEK: Sulfonated Poly Ether Ether Ketone.
[f] PES: Polyether sulfone.
[g] PVDF: Polyvinylidene Fluoride.
[h] CHI/CNT hydrogel: a screen-printed carbon electrode coated with multi-wall carbon nanotube and chitosan hydrogel composite.
[i] PAN: Polyacrylonitrile.
[j] the type of PEM did not mention in the study.

around the hollow fiber. The anodic carbon cloth was tightened by a copper wire as the anodic current collector to transmit the produced electrons to the external circuit. Carbon cloth facilitates electron transfer and creates the appropriate condition for the growth of bacteria. The cathode electrode was the single copper wire inside the hollow fiber that was connected to the external circuit. The schematic representation of the hollow fiber-MFC design and the image of three identical MFC set-ups have been illustrated in Fig. 1 (A) and (B), respectively.

Anaerobic wastewater from the sewage treatment plant of Sistan and Baluchestan University (Zahedan, Iran) was continuously pumped (3.5 ml/ min, ca. 35 ± 2 °C) as the anodic electrolyte solution without any inoculation period or addition of any supplementary nutrients or salts. Chemical analysis results of the influent wastewater is available in Table S1, in the supplementary data (Appendix A). Tap water was aerated using an air pump and constantly fed to the cathode chamber as the cathode electrolyte to provide sufficient oxygen for the cathodic reaction. The carbon cloth electrodes were cleaned after each experiment by firstly dipped in HCL solution (1 M, for 1 h), then after twice rinsing with DI water, they were soaked in NaOH solution (1 M, for 1 h) and placed in DI water before reusing in the later experiment. The copper wires of the anode and cathode electrodes have been replaced after each experiment. Experiments were conducted at ambient temperature (30–35 °C) and performed three times to ensure reproducibility and minimize the contribution of errors and possible changing the environmental conditions to the results.

2.2. Analysis and calculations

The open circuit voltage (OCV) and the close circuit voltage (CCV) were measured by a digital multi-meter at 15-minute intervals and using an external resistor load of 1000 Ω (R_{ex}).

After reaching the stable conditions, the polarization curve was obtained by varying the external resistances from 46,000 to 10 Ω. The resulting voltage at each resistor was recorded when it stabilized. Current (I=CCV/R_{ext}, mA) and power (P=I × CCV, mW) generation of the MFCs were calculated according to Ohm's law and normalized by the external surface area of the hollow fiber membrane. The efficiency of wastewater treatment was determined by comparing the chemical oxygen demand (COD) and Biological oxygen demand (BOD) of the inlet and outlet wastewaters using the COD measurement instrument (AL250 Photometer and AL38 CSB/COD-Reactor, AQUALYTIC, Germany), and Manometric BOD Measuring Device (OxiTop® IS, USA), respectively. The coulomb efficiency (CE) was defined as the ratio of electron recovery from the influent organic matter, which was calculated as described previously [45,51,52,54,56]. Scanning electron microscopy (LEO 1455VP) analysis was performed to observe the surface and cross-section morphology of the implemented hollow fiber membranes.

2.3. Oxygen diffusion coefficient

The oxygen mass transfer coefficient (ko) was determined by measuring the dissolved oxygen concentration (YSI 5100 Incorporated, Ohio, USA) of abiotic MFCs over time. Before the measurement, the entering DI water in the anode chamber should be deoxygenated via sparging nitrogen gas, whereas the cathode chamber is continuously fed by aerated DI water. Considering the small volume of the anode compartment of the MFCs, the outlet of the anodic chamber entered a sealed container that was equipped with a DO probe to measure the average dissolved oxygen (mixing cup). The oxygen concentration in the cathode chamber was normally stable at the saturated concentration owing to the aeration. The oxygen mass transfer coefficient (Ko_2, cm. s^{-1}) was determined using the monitored DO values by Eq. (1):

$$k_{O2} = \frac{V}{At} ln\left[\frac{C_{O2@cathode} - C_{O2@anode}}{C_{O2@cathode}}\right] \quad (1)$$

where V (cm^3) represents the anodic volume, A (cm^2) is the cross-sectional area of the hollow fiber membrane, $C_{O2@cathode}$ and $C_{O2@anode}$ ($mg.l^{-1}$) are the saturated dissolved oxygen in the cathode chamber, and oxygen concentration in the anode chamber at time t, respectively [51,54,56,73]. The oxygen diffusion coefficient (D_{O2}, $cm^2.s^{-1}$) was calculated by Eq. (2) as follows:

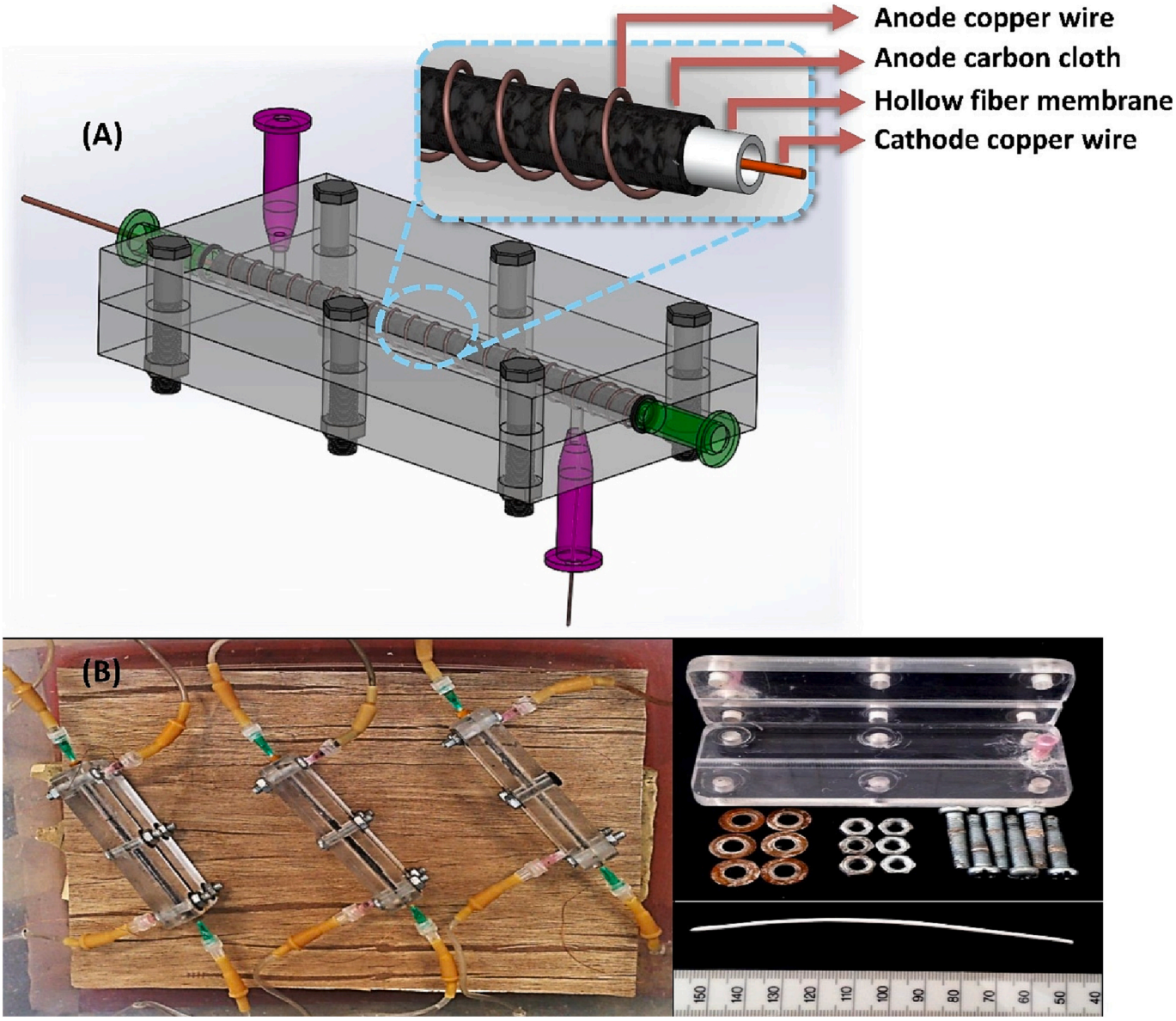

Fig. 1. (A) The 3D representation of the milliliter scale MFCs, (B) the set-up picture of the utilized MFCs (three identical MFCs in each experiment placed in the adjusted temperature box) accompanied by the constituent parts of the MFCs including the drilled plexiglass, nuts and bolts, and hollow fiber membranes.

$$D_{O2} = k_{O2} \times L \quad (2)$$

where L (cm) is the thickness of hollow fiber membranes.

2.4. Electrochemical investigation of MFCs

Cyclic voltammetry (CV) analysis was implemented from −1.1 to 1.0 V with a scan rate of 0.1 V s^{-1} using the Autolab PGSTAT302N High-Performance potentiostat instrument (Metrohm, Netherland) between the anode and cathode electrodes. The Internal resistance components, such as the ohmic and charge transfer resistances of the MFCs with different PEM at the stable voltage generation, were determined using the electrochemical impedance spectroscopy (EIS) technique. The frequency range of 0.1 Hz to 100 kHz with a voltage amplitude of 0.1 V was applied in the two-electrode AC method of EIS analysis. The EIS was performed twice for each experiment to ensure the reproducibility of data. Firstly, the anode electrode was implemented as the working electrode, and the cathode served as both the counter electrode and reference electrode [74,75]. Then the working and counter electrodes were reversed. The obtained results were investigated by fitting an Equivalent circuit model on the spectra using NOVA 1.11 software, and the average and standard deviations of internal resistance components have been reported. The proton conductivity of the membranes can be calculated according to EIS results. The conductivity of the membranes (σ, S/cm) was determined by Eq. (3):

$$\sigma = \frac{L}{R_s * A} \quad (3)$$

where L, A, and R_s represent the membrane thickness (cm), the surface area of the membrane (cm^2), and the ohmic resistance according to EIS data (Ω), respectively [51,52,54,56,76].

3. Results and discussions

In the present study, three different polymeric hollow fiber types were examined as the proton exchange membrane of milliliter-scale MFCs. The performance of these MFCs was investigated regarding the electricity generation and wastewater treatment capabilities.

3.1. The characterization of the hollow fiber membranes

Scanning electron microscopy (SEM) was employed to observe the surface and cross-section morphology of the utilized commercial hollow fiber membranes. The cross-section SEM images of the PES membrane (Fig. 2 A and B) reveal a highly porous and void internal structure between the two more dense surface layers. Moreover, the surface SEM of PES (Fig. 2 C) indicates an evenly uniform distributed porosity with an average pore size of 200 nm, which can provide vast proton conductivity and high oxygen permeability for this polymeric membrane. Fig. 2 D and E represent the cross-sectional images, and Fig. 2F indicates the surface image of the PAN hollow fiber membrane. The cross-sectional and surface SEM images of PVDF are exhibited in Fig. 2 G, H, and Fig. 2 I, respectively. The PAN (Fig. 2 D, E, F) and the PVDF membranes (Fig. 2 G, H, I) exhibit denser cross-sectional and surface structures compared to PES. Seemingly, the highly porous structure of PES hollow fiber could improve the membrane performance in terms of water sorption and proton conduction and thereby provides more efficient proton transportation through the membrane from the anode to the cathode chamber. On the other hand, the performance of the MFCs could be impressed by the excess oxygen permeation through the greatly porous PES membrane. High oxygen diffusion from the cathode to the anode chamber could decrease the coulombic efficiency and electricity generation of the MFCs owing to the occurrence of aerobic respiration of nutrients in the anode and the extinction of the anoxic anodic environment, which is critical for the growth of *exo*-electrogenic bacteria.

Furthermore, the wettability of the hollow fiber proton exchange membranes was investigated by contact angle measurement. As shown in Fig. 3, the PES membrane exhibited the lowest contact angle of about 43.5° due to the presence of hydrophilic sulfone polar groups on its structure. After that, the PAN membrane is a more hydrophilic membrane with a contact angle of 66° compared to PVDF, with a contact angle of 87°. Better absorption of water droplets on the membrane surface can improve the proton conductivity of membranes by the vehicular mechanism.

The oxygen permeability of each separator was measured in terms of their mass transfer coefficients (k_{O2}, cm/s) and diffusion coefficients (D_{O2}, cm^2/s), as summarized in Table 2. The oxygen mass transfer coefficient values for all three implemented separators in this study are in the acceptable range for MFC application and comparable with the values reported for the Nafion 117 (1.72×10^{-4} cm/s [77], 2.77×10^{-4} cm/s [78], 1.3×10^{-4} cm/s [33], 2.05×10^{-4} cm/s [79], 3.6×10^{-4} cm/s [80]). As expected, PES has the highest oxygen diffusion rate owing to its more porous structure and the further hydrophilicity due to the p + resence of the polar sulfone group on its chemical structure. The PAN membrane has second place, and the PVDF membrane exhibits the lowest oxygen transfer coefficient due to the dense structure and higher thickness of the membrane. Table 2 compares the physical specifications of the membranes briefly.

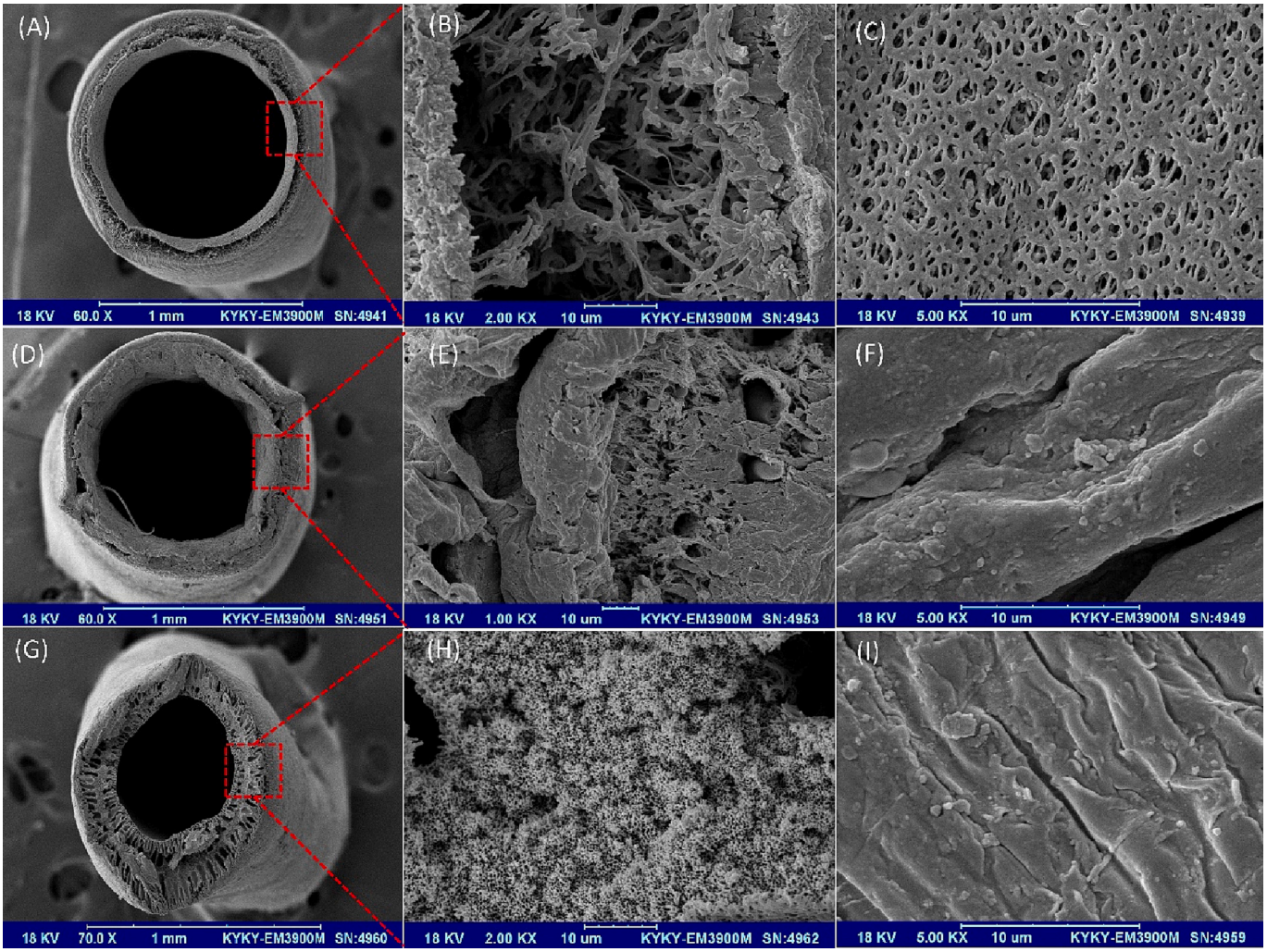

Fig. 2. SEM images of hollow fiber membranes; the first and the second columns from left represent the cross section with different resolutions, and the third column is attributed to the surface SEM images; PES (the first row (A, B, C)), PVDF (the second row (D, E, F)), and PAN (the third row (G, H, I)).

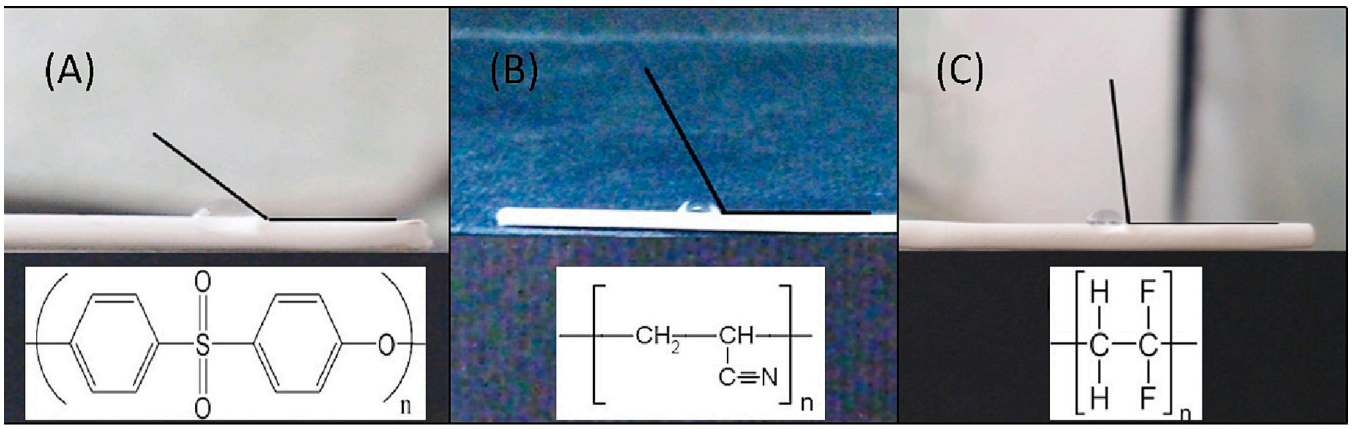

Fig. 3. The water contact angle of different hollow fiber membranes accompanied by their chemical structures; (A) PES, (B) PAN, (C) PVDF.

Table 2
The comparison of the physical properties of different hollow fiber membranes utilized in this study.

Membrane type	Thickness (mm)	Pore size (nm)	Outer diameter (mm)	Contact angle (°)	D $_{O2}$*10^{-6} (cm^2/s)	K $_{O2}$* 10^{-4} (cm/s)
PES	0.1	200	1	43.5	4.2	4.2
PAN	0.175	30	1	66	3.99	2.28
PVDF	0.28	30	1.3	87	3.33	1.19

3.2. The electricity generation performance

The increasing trends of open circuit voltage (OCV) and the current generation of the hollow fiber-based MFCs during the start-up period are depicted in Fig. 4 A and B, respectively. Moreover, the current generation of each membrane are separately represented in Fig. S1 in the supplementary data (Appendix A). Furthermore, the performance of the MFCs based on the electricity generation capabilities is summarized in Table 2. The maximum obtained OCV values for PES, PAN, and PVDF are in the same ranges, and no significant differences are observed between the voltage generation of these three hollow fiber membranes (*P*-value>0.05). It can be concluded that since all conditions are the same, the mechanism of electron production remains unchanged, so there is no considerable difference in the OCVs, and they have similar patterns.

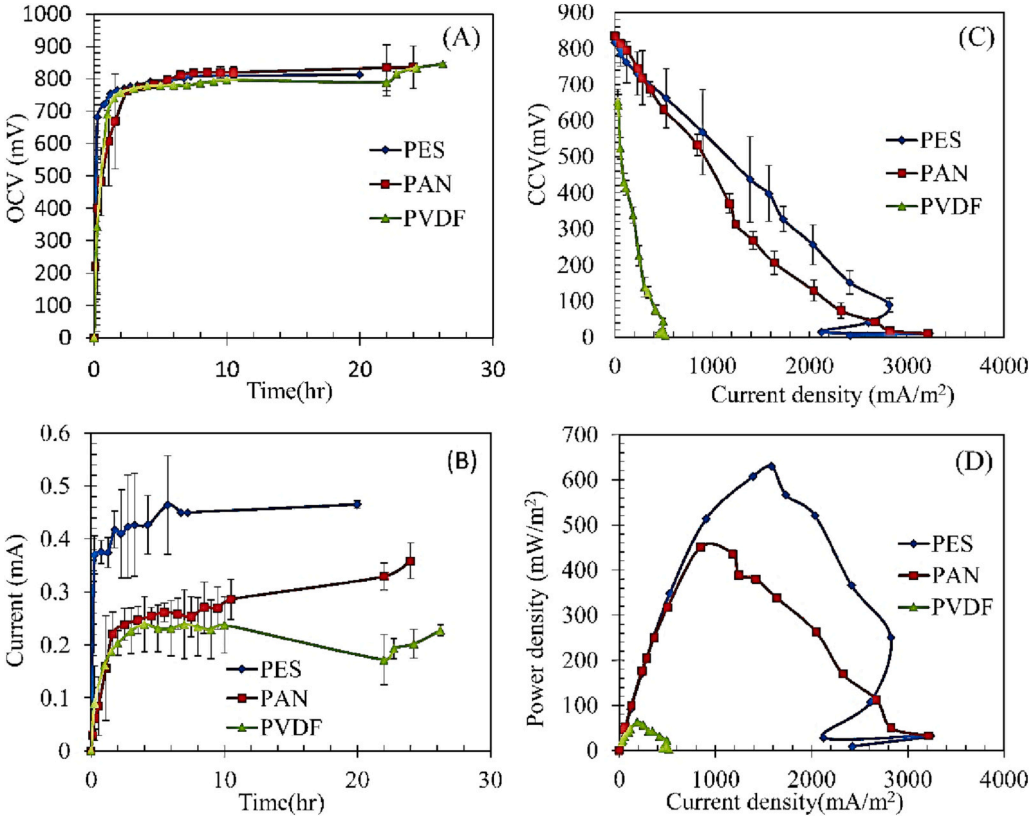

Fig. 4. The electricity generation and polarization results of the hollow fiber-based MFCs: (A) open circuit voltage (OCV) versus time and (B) current generation curve, (C) and (D) polarization test results.

Also, the time to reach stability for all three membranes is almost the same, and the system reaches stable condition after about 2.5 h.

However, the maximum current generations of 0.46, 0.35, and 0.22 mA are obtained for PES, PAN, and PVDF, respectively, which are statistically different (P-value<0.05). Seemingly, the highly porous structure accompanied by the great hydrophilicity of the PES membrane resulted in the appropriate proton conductivity, which is of great importance for the efficient electricity generation performance of MFCs. Also, the current generation proficiency of the other two hollow fiber membranes is directly related to their porosity, wettability, and proton conduction properties.

Fig. 4C and D exhibit the polarization curves for all three membranes. Although an in-depth investigation of the internal resistance components is performed in section 3–5 by interpretation of the EIS results, a quick observation of the slope of the polarization curve (Fig. 4C) could provide a rough estimate of the internal resistance value for the MFCs. The highest slope is observed for the PVDF membrane (ca. R_{in} = 2763 Ω), then the PAN and PES membranes with the internal resistance of about 1818 and 759 Ω are in the second and third places, in turn. The internal resistance of the MFC systems depends on various factors, including the design-related parameters such as the electrode's types and spacing and the types of separating membrane, as well as the other reaction-influencing parameters like the microorganism's spectra, substrate, and so on. Because the only distinction between the present MFC systems was in the type of separators, different internal resistances most likely occurred due to the disparate proton transfer rates of membranes. Membrane thickness and porosity affect the permeability of a membrane to the protons, substrate, and oxygen molecules. The thicker and denser the membrane, the higher the internal resistance observed. According to the reported thickness, porosity, and hydrophilicity of the membranes (Table 2), the internal resistance is conversely related to the proton conduction capability of the membranes.

Fig. 4 D shows the power density curve versus the current density during the polarization test. The PES generated the highest power and current densities compared to the PAN and PVDF membranes. This superior power generation performance was likely acquired due to its greater proton conductivity of PES. However, a sharp reduction of current density was observed at the high current values of the polarization curve for the PES membrane owing to mass transport overpotential. This phenomenon occurs because of restricted mass transfer of chemical species, i.e., the lack of reactants supply or accumulation of products nearby the electrode's surface due to the high rate of reactions or limited geometry of reactors. Hence, the diffusion of species to or from the reaction zone impedes the current generation and results in mass transport overpotential at the high current density part of the polarization curve [81]. The maximum output power and current densities under continuous flow conditions are also summarized in Table 3. Moreover, the coulombic efficiency of each MFC system, which is calculated by the produced current versus time integral, is reported in Table 3. As can be seen, the coulombic efficiency of the MFCs with different hollow fiber membranes is in the same order of magnitude.

3.3. Wastewater treatment efficiency

The wastewater treatment quality of the hollow fiber-based MFCs was evaluated based on the COD removal efficiencies (Table 3). The influent wastewater has a natural pH range (7 ± 0.5), an average COD value of 540 mg/l, and an electrical conductivity of 1.98 ± 0.42 mS/cm, which are considered constant for all the experiments. As mentioned in Table 3, the COD removal efficiency is relatively low for all the employed separators in the present hollow fiber-based MFC design. Various MFC designs are available for different applicability, and milliliter scale MFCs do not implement for wastewater treatment applications. Nevertheless, they could be a suitable choice for bio-sensing utilizations.

Considering the COD concentration of the influent wastewater in the present research, a sufficient nutrient is available for microorganism metabolism. Nonetheless, because of the small anodic volume and short hydraulic retention time (about 1 min), there is not enough time and space for the anodic microorganism to degrade the influent substrates sufficiently. The highest COD removal efficiency was obtained by the PES membrane (11.48 %), and the PVDF resulted in the lowest performance (6.48 %). The lower COD removal of PVDF may be because of a probable pH splitting in the anode chamber, owing to limited proton conductivity, which can seriously hinder the normal metabolism of anodic microorganisms.

3.4. Cyclic voltammetry (CV)

The cyclic voltammetry (CV) analysis was applied to evaluate the electron transfer mechanism and microbial electrogenic activity. The results of CV analyses for the MFCs operated with the different membranes are shown in Fig. 5. As can be seen, the CV voltammograms for all the MFCs have a relatively similar sigmoidal shape without observable current peaks, except for two feeble oxidative humps at −800 mV and 400 mV for the PES membrane. The PES membrane resulted in a higher oxidative anodic current peak of 3.39 mA compared to the PAN and PVDF membranes, with 2.27 mA and 1.02 mA, respectively. Likewise, the cathodic half cycles of the PES, PAN, and PVDF membranes generated the redox current peaks of −2.45 mA, −2.00 mA, and $-6.42*10^{-4}$ mA, respectively. The higher oxidative and redox peaks for PES could be attributed to its superior charge transfer, which is in good agreement with the electricity generation results. Moreover, the higher difference between the oxidation and reduction half cycles of CV voltammograms for the PES compared to the PAN and PVDF membranes reveals its higher capacitive nature, probably due to the presence of thicker electrogenic biofilm in the anodic half-cell.

3.5. Electrochemical impedance spectroscopy (EIS)

Two-electrode configuration of EIS analysis was performed at least twice for each experiment to assess the internal resistance components of the MFC systems. The equivalent electrical circuit (EEC) modeling was used to analyze the experimental EIS data. The implementation of a well-chosen EEC could provide a suitable model for estimating the internal resistance constituents and investigating the vital influencing factors on the MFC performance. The EEC model includes distinctive electrical elements selected based on the types and design of electrodes and the geometrical specification of the MFC system [74,75]. In the present study, the polarization impedance of the electrodes has been defined by a modified Randle circuit which involves the parallel combination of charge transfer resistance (R_{ct}) and a constant phase element (CPE) for the non-ideal capacitance of the electrical double-layer adjacent to the electrodes. In the case of the anode electrode, a Gerischer

Table 3
The electricity generation and wastewater treatment proficiency of the hollow fiber-based MFCs.

Hollow fiber Membrane	OCV (mV)	Current (mA)	Max power density (mW/m^2)	Max current density (mA/m^2)	Coulombic efficiency (%)	COD out (mg/l)	COD removal (%)
PES	813	0.46	629	1333	4.22	478	11.48
PAN	836	0.35	450	847	3.49	483	10.55
PVDF	845	0.22	63	187	3.12	500	6.48

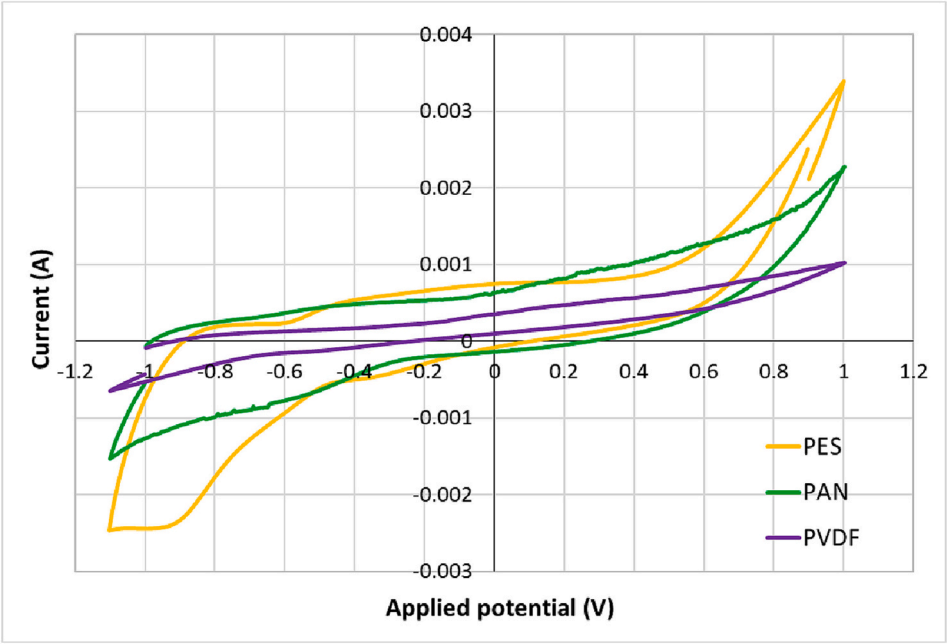

Fig. 5. Cyclic voltammograms for different polymer-based MFCs.

element was added in series by the R_{ct} to assimilate the combined occurrence of diffusion and reaction phenomena in the porous carbon cloth electrode. The resistor of R_s indicates the ohmic losses of the hollow fiber membranes and electrolyte solutions [51,52,54]. Fig. 6 A illustrates the EEC model which is proposed in the present research. The experimental EIS data were fitted using NOVA software by minimizing

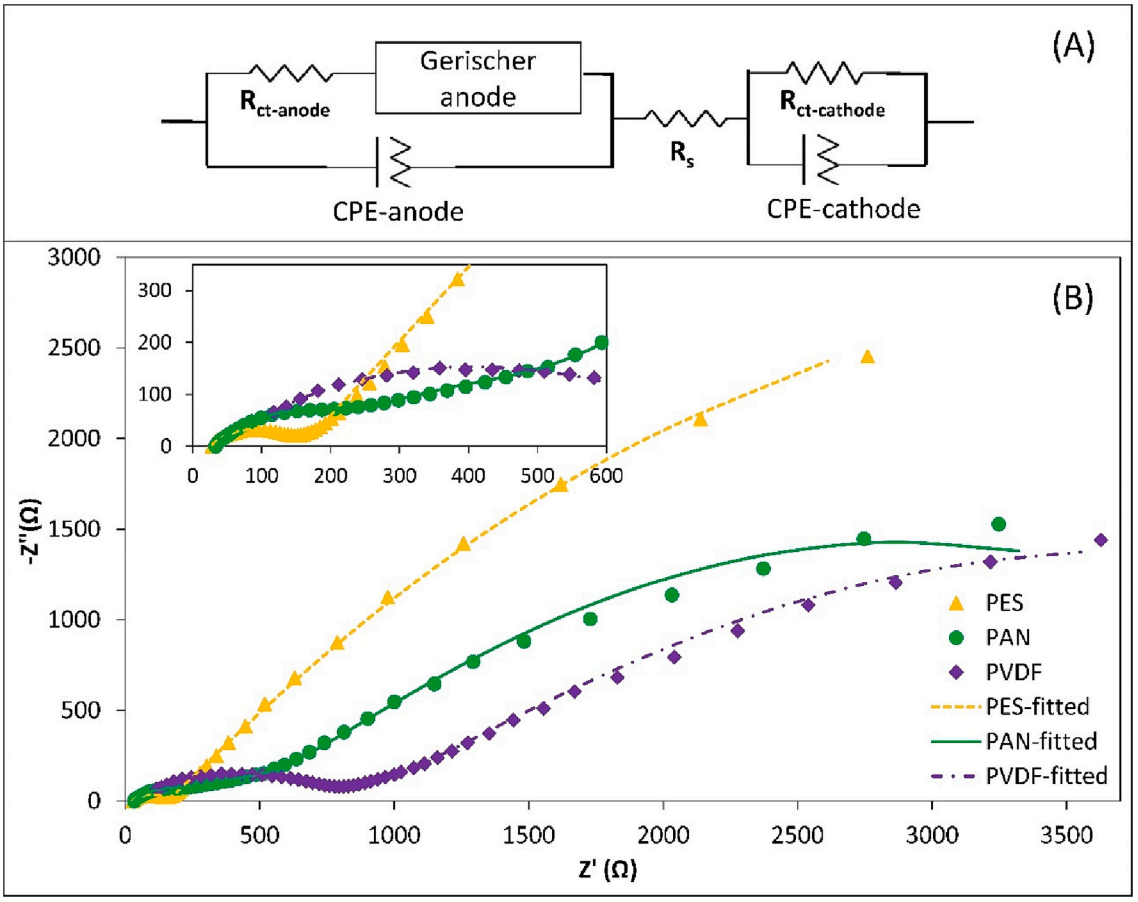

Fig. 6. (A) the proposed equivalent electrical circuit for the simulation of the MFC systems; (B) the results of EIS analysis for the hollow fiber-based MFCs, the lines indicate the fitted values on the experimental data (markers); the inset exhibits the high-frequency section of Nyquist plots with higher resolution.

the chi-square (χ^2) parameter and implementing the *Kramers-Kronig* test to investigate the sufficient compliance of the EIS data. The diminutive values of chi-square (χ^2) that were obtained for the simulation (lower than 10^{-3}) and the *Kramers-Kronig* test (lower than 10^{-6}) authenticate the accuracy of modeling. Fig. 6 B represents the experimental (markers) and the fitted (lines) Nyquist plots of the MFCs.

Table 4 tabulates the results of EEC modeling for each MFC. As expected, the values of ohmic resistance (R_s, Ω) for all the hollow fiber-based MFCs are lower than the values of anodic and cathodic charge transfer impedances. Seemingly, the slight thickness of hollow fiber membranes (Table 2) adequately closed the gap between the anode and cathode electrodes and diminished the ohmic resistance. The PES membrane has the lowest ohmic resistance and the highest proton conductivity among the others. It could be attributed to its larger pore size and the presence of a sulfonate functional group in its chemical structure, which resulted in the higher hydrophilicity and proton conductivity of PES hollow fiber. The PAN and PVDF membranes have the second and the third proton conductivity values afterward (Table 4).

The PES membrane has the minimum anodic charge transfer resistance (R_{cta}) owing to its superior proton conductivity. Thereafter, PAN and PVDF membranes caused 1.59 and 3.2 times higher anodic charge transfer impedances than the PES, respectively. The greater proton conductivity of a membrane boosts the growth and propagation of *exo*-electrogenic bacteria and thereby facilitates the anodic electron transfer using their conductive pillis. In this context, Palanisamy et al. (2023) explained that the incorporation of sulfonated inorganic additives into the polymeric membrane of MFCs could vastly promote the proton conductivity via the vehicular (diffusion) and Grotthuss (hopping) mechanisms owing to the presence of sulfonate functional group [82].

Furthermore, the cathodic charge transfer impedances (R_{ctc}) of the hollow fiber membranes have a similar trend to the anodic charge transfer resistance. Therefore, the proton conductivity of the membranes not only affected the anodic reaction proficiency but also notably influenced the cathodic oxygen reduction reaction (ORR) performance.

The electrical double layer in the proximity of the electrodes has been simulated by the constant phase element (CPE). CPE denotes a heterogeneous capacitor that occurred due to the biofilm formation with pseudo-capacitive features or unevenness of the electrode surface. The CPE impedance is described using two frequency-independent constants of α and Q ($F.s^{\alpha-1}$ or $S.s^{\alpha}$) and calculated by the following equation (Eq. (4)):

$$Z_{CPE}(\omega) = \frac{1}{(j\omega)^{\alpha} Q} \tag{4}$$

where j and ω are the imaginary unit ($j = \sqrt{-1}$) and the angular frequency, respectively. In the case of EDL simulation, it was shown that Q has a direct relationship with the capacitance of EDL, which is raised as a result of biofilm thickening. Moreover, α is related to the maturation of biofilm nearby the electrode [54]. However, regarding the complexity of the physical interpretation of the CPE element, several models and equations have been proposed to estimate the effective capacitance of EDL using the CPE parameters. Here, the equation proposed by Brug et al. [83] is applied (Eq. (5)).

$$C_{DL} = \left[Q \left(R_s^{-1} + R_{ct}^{-1} \right)^{(\alpha-1)} \right]^{1/\alpha} \tag{5}$$

where C_{DL}, R_s, and R_{ct} are the effective capacitance, ohmic, and charge transfer impedances of the electrode. As can be seen in Table 4, the C_{DL} value for the anodic EDL of the PES membrane (349.73 ± 21.53 μF) is 25.5 times higher than the value of the PAN membrane and 1520.5 times greater than the PVDF hollow fiber. This extremely larger value of anodic EDL effective capacitance compared to the other membranes could be attributed to its greater proton conductivity, which boosted the growth of electrogenic bacteria over the electrode. The pseudo-capacitive characteristic of c-type cytochromes on the bacterial cell membrane raised the capacitance and reduced the anodic charge transfer impedance, consequently. Several researches verified that increasing the anode capacitance has substantial effect on the stabilization and enhancement of current and power output of the MFCs [75]. For instance, Fang et al. (2022) reported that increasing the thickness of the assembled *Shewanella* biofilm resulted in the enhanced anodic capacitance, and thereby improved power output, despite of augmented internal resistance. They concluded that the effect of capacitance on current generation could be more conspicuous than the resistance of thick biofilm [84].

The cathodic EDL capacitance of all the membranes is notably lower than the anodic EDL by about three orders of magnitude. The large differences between the quantity of anodic and cathodic C_{DL} occurred because of the distinctive type and design of the electrodes. Porous carbon cloth as the anode electrode provides an appropriate environment for the growth of bacteria and causes a high capacitive nature for the anode electrode. In comparison, implementing a single copper wire as the cathode electrode could not form a thick EDL near the electrode, even if the microorganisms existed in the cathodic chamber.

The accompanied incidence of diffusion and reaction in the porous structure of carbon cloth anode is simulated by Gerischer element, which is described by the following equation (Eq. (6)):

$$Z_G(\omega) = \frac{1}{Y_0 \sqrt{k + j\omega}} = \frac{R_d}{\sqrt{k + j\omega}} \tag{6}$$

where Y_0 (S) and R_d (Ω) represent the diffusional admittance and impedance of the Gerischer element, respectively, and k indicates the overall rate constant of the anodic electrode reactions. The diffusional resistance of the anodic half-cell has been determined by reversing the obtained admittance. The diffusional impedance (R_d) has a maximum value of 163.8 ± 17.9 Ω for the PES membrane, a mediocre value of 142.63 ± 10.64 Ω for the PES, and a minimum quantity of 63.74 ± 3.48 Ω for PVDF hollow fiber. Seemingly, the diffusional resistance is conversely related to the density and thickness of anodic biofilm.

Furthermore, the overall anodic reaction rate (k-Gerischer) has the maximum value for the PES membrane, which is caused by the higher activity of *exo*-electrogenic bacteria in the anode chamber of this MFC system. The PAN membrane has the second reaction rate, and the PVDF separator has the minimum reaction rate value due to its lowest proton conductivity.

Table 4
The fitted values of equivalent electrical circuit elements.

Membrane	Rs (Ω)	σ (mS/cm)	R_{cta} (Ω)	R_{ctc} (Ω)	CPE-anode			CPE-cathode			Gerischer-anode		
					$Q \times 10^{-5}$	α	C_{DL} (μF)	$Q \times 10^{-5}$	α	C_{DL} (nF)	$K \times 10^{-3}$	$Y0 \times 10^{-4}$ (S)	R_d (Ω)
PES	24.86 ± 0.07	128.10 ± 0.37	175.33 ± 18.97	131.58 ± 8.65	180.24 ± 16.32	0.66 ± 0.01	349.73 ± 21.53	2.70 ± 0.30	0.57 ± 0.005	107.07 ± 8.05	41.06 ± 0.76	65.1 ± 2.37	163.8 ± 17.9
PAN	31.73 ± 0.47	100.39 ± 1.49	279.08 ± 13.12	247.04 ± 35.82	14.17 ± 2.35	0.70 ± 0.027	13.71 ± 0.99	1.34 ± 0.50	0.64 ± 0.02	139.07 ± 7.48	37.26 ± 3.56	70.3 ± 5.25	142.63 ± 10.64
PVDF	33.29 ± 0.36	73.59 ± 0.8	561.23 ± 16.52	657.31 ± 7.43	57.11 ± 1.59	0.34 ± 0.009	0.23 ± 0.05	0.29 ± 0.008	0.51 ± 0.002	0.40 ± 0.001	23.81 ± 5.32	157.1 ± 8.58	63.74 ± 3.48

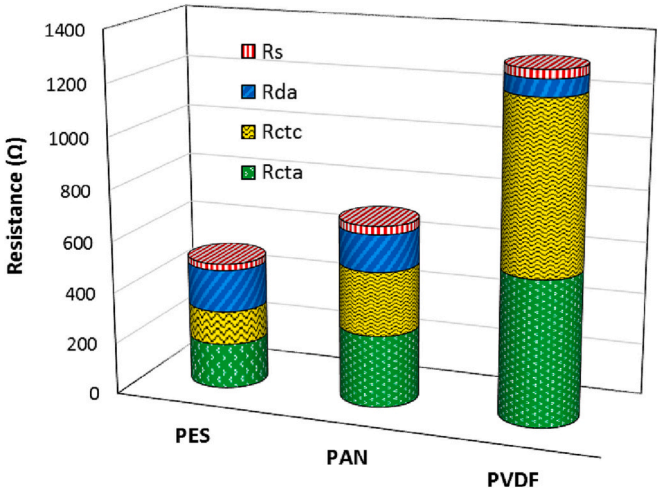

Fig. 7. The components of internal resistance for three hollow fiber-based MFCs. Rs: ohmic resistance, Rda: diffusional resistance of anode, Rctc: charge transfer resistance of cathode, Rcta: charge transfer resistance of anode electrode.

Finally, the internal resistance components of the hollow fiber-based MFCs have been compared graphically in Fig. 7. The PES-based MFC has shown the lowest internal resistance of 495.57 Ω, the PAN membrane with an internal resistance of 700.47 Ω was the second one, and the PVDF has gained the highest internal resistance of 1315.57 Ω. Evidently, the ohmic resistance was the smallest part (2.5 to 5 %) of internal resistance for all the hollow fiber-based MFCs due to their small thickness. The major differences between the internal resistance were attributed to the charge transfer impedances of electrodes.

4. Cost analysis

The economic investigation is one of the main topics of concern for the commercialization of each technology. The cost and the power output of the utilized hollow fiber membranes are compared with the other separator types in Table 5. All the introduced hollow fiber membranes, particularly the PES and PAN membranes, have generated a greater power output than the expensive Nafion membrane. Of course, a thorough comparison with other MFC studies in the literature is unattainable due to the vast difference in size, configuration, membrane type, substrate, and experiment conditions. However, the obtained results have shown an apparent potential of polymeric hollow fiber membranes for power production in MFC systems.

5. Conclusion

The performance of a novel milliliter-scale MFC using three different low-cost hollow fibers of PES, PAN, and PVDF has been examined in the present study. The PES-based MFC exhibited the highest power and current generation performance compared to PAN and PVDF membranes. Having sulfonic groups in the polymeric backbone, better wettability and a highly porous structure resulted in the superior proton conductivity of the PES hollow fiber membrane. Moreover, the EIS data have been analyzed using the equivalent electrical circuit modeling method to individualize the components of internal resistance. The MFC system was modeled using a resistor for the ohmic losses and two resistors for the charge transfer impedances of the electrodes, which were connected in parallel with a constant phase element (CPE) for simulating the non-ideal capacitance of electrical double layers (EDL) near the electrodes. Moreover, a Gerischer element (G) assimilate the coupled diffusion and reaction occurrence in the porous anode electrode. According to the results, the ohmic resistance constitutes only 2.5 to 5 % of the internal resistance of hollow fiber-based MFCs because of the very short distance between the electrodes. The PES exhibited the lowest ohmic impedance owing to its higher proton conduction capability. However, the major differences between the internal resistance of the MFCs have been attributed to the charge transfer impedances of the electrodes. A better propagation of anodic electrogene bacteria as a result of appropriate proton conduction of the PES membrane raised the capacitance of EDL and reduced the charge transfer impedance of the anode electrode. However, the diffusional impedance of the anode electrode has been slightly elevated in a thick anodic biofilm.

Based on the COD removal efficiencies, these small hollow fiber-based MFCs have not been very prosperous in wastewater treatment because of their small anodic chamber volume (2.75 ml). However, the distinctive specifications, including the short electrode distance, acceptable power output, and fast response time, make the proposed milliliter-scale MFC a promising option for bio-sensing applications. In future studies, the MFC stack's feasibility could be assessed for providing the required power for small utilities.

Table 5
A comparison of power output and cost of the present hollow fiber membranes with the other separator types.

Membrane	CD_{max} (mA/m^2)	P_{max} (mW/m^2)	Cost (US $\$/m^2$)	Power output (mW/ US $)	Reference
PES	1333	629	40	15.73	This study
PAN	847	450	33	13.64	This study
PVDF	187	63	33	1.91	This study
Nafion 117	310	118	2300	0.05	[57]
Nafion 117	1750	602	2300	0.26	[85]
Low-cost organic membrane (LCM)	1.24 ± 0.15(mA)	61 ± 14	14	4.36	[86]
Nafion 117	3.19 ± 0.23(mA)	403 ± 58	1733	0.23	
SPEEK (DS = 63.6 %)	287	68.64	375	0.18	[87]
Nylon cloth+ j-cloth+ glass fiber	1414.43	281.30	7.32	38.43	[45]
SBC with PVA	224.86	41.8	77	0.54	[73]
PVA-Nafion borosilicate	800 (mA/m^3)	6800 (mW/m^3)	151	….	[88]
PPS	~ 410	102	8.33	12.24	[89]
SPPS	~ 1100	190	9.2	20.65	
PP100	~ 1350	117	0.57	205.26	
CMI-7000	~700	78	166	0.47	
Nafion 117	~160	24	2300	0.01	
AEM	~1500	449 ± 35	80	5.6	[39]

SBC: Sulphonated biochar, PPS: Polyphenylene sulfide, SPPS: Sulfonated Polyphenylene sulfide, PP: Polypropylene, SPEEK: Sulfonated Poly Ether-Ether Ketone.

Declaration of competing interest

The authors declare that they have no known competing financial interests or personal relationships that could have appeared to influence the work reported in this paper.

Data availability

Data will be made available on request.

Acknowledgment

This research was supported by the University of Sistan and Baluchestan (Grant number 932/2/1006).

Appendix A. Supplementary data

Supplementary data to this article can be found online at https://doi.org/10.1016/j.jwpe.2023.104064.

References

[1] H. Wang, et al., Bioelectrochemical system platform for sustainable environmental remediation and energy generation, Biotechnol. Adv. 33 (3–4) (2015) 317–334.
[2] M. Rahimnejad, et al., Microbial fuel cell as new technology for bioelectricity generation: a review, Alex. Eng. J. 54 (3) (2015) 745–756.
[3] B.E. Logan, et al., Microbial fuel cells: methodology and technology, Environ. Sci. Technol. 40 (17) (2006) 5181–5192.
[4] B.E. Logan, Microbial Fuel Cells, John Wiley & Sons, New Jersey, 2008.
[5] A. Naderi, et al., Putting the electro-bugs to work: a systematic review of 22 years of advances in bio-electrochemical systems and the parameters governing their performance, Environ. Res. 229 (2023), 115843.
[6] S.V. Ramanaiah, et al., Bioelectrochemical systems (BESs) for agro-food waste and wastewater treatment, and sustainable bioenergy-a review, Environ. Pollut. 325 (2023), 121432.
[7] D. Bhowmik, et al., Multitudinous approaches, challenges and opportunities of bioelectrochemical systems in conversion of waste to energy from wastewater treatment plants, Clean. Circ. Bioeconomy 4 (2023), 100040.
[8] T. Kouam Ida, B. Mandal, Microbial fuel cell design, application and performance: a review, Mater. Today Proc. 76 (2023) 88–94.
[9] Q. Wu, et al., Microbial fuel cell system: a promising technology for pollutant removal and environmental remediation, Environ. Sci. Pollut. Res. 27 (7) (2020) 6749–6764.
[10] B.E. Logan, Exoelectrogenic bacteria that power microbial fuel cells, Nat. Rev. Microbiol. 7 (5) (2009) 375–381.
[11] M.R. Sulaiman, R.K. Gupta, Recent Advances in Microbial Fuel Cells for Sustainable Energy, in Sustainable Energy Storage in the Scope of Circular Economy, 2023, pp. 183–201.
[12] T. Kouam Ida, B. Mandal, Microbial fuel cell design, application and performance: a review, Mater. Today Proc. 76 (1) (2022) 88–94.
[13] R. Rossi, B.E. Logan, Impact of reactor configuration on pilot-scale microbial fuel cell performance, Water Res. 225 (2022), 119179.
[14] T. Naaz, et al., Recent advances in biological approaches towards anode biofilm engineering for improvement of extracellular electron transfer in microbial fuel cells, Environ. Eng. Res. 28 (5) (2023).
[15] D. Vidhyeswari, A. Surendhar, S. Bhuvaneshwari, General aspects and novel PEMss in microbial fuel cell technology: a review, Chemosphere 309 (2022), 136454.
[16] J.X. Leong, et al., Ion exchange membranes as separators in microbial fuel cells for bioenergy conversion: a comprehensive review, Renew. Sust. Energ. Rev. 28 (2013) 575–587.
[17] A. Paitier, et al., Effect of contact area and shape of anode current collectors on bacterial community structure in microbial fuel cells, Molecules 27 (7) (2022) 2245.
[18] P.A. Opoku, et al., Scaled-up multi-anode shared cathode microbial fuel cell for simultaneous treatment of multiple real wastewaters and power generation, Chemosphere 299 (2022), 134401.
[19] O. Prakash, et al., A novel design for the development of deployable benthic microbial fuel cells using PPy-Fe2O3 coated multi-anode system, Sustain. Energy Technol. Assess. 52 (2022), 102049.
[20] Y. Zhu, et al., Economic affordable carbonized phenolic foam anode with controlled structure for microbial fuel cells, Sci. Total Environ. 810 (2022), 151314.
[21] L. Meng, et al., High-performance free-standing microbial fuel cell anode derived from Chinese date for enhanced electron transfer rates, Bioresour. Technol. 353 (2022), 127151.
[22] S. Jin, et al., Three-dimensional N-doped carbon nanotube/graphene composite aerogel anode to develop high-power microbial fuel cell, Energy Environ. Mater. 6 (3) (2023) e12373.
[23] S. Qian, et al., Tuning electrospinning hierarchically porous nanowires anode for enhanced bioelectrocatalysis in microbial fuel cells, Nano Res. 15 (6) (2022) 5089–5097.
[24] B. Tripathi, et al., Modification of graphite sheet anode with Iron (II, III) oxide-carbon dots for enhancing the performance of microbial fuel cell, Catalysts 12 (9) (2022) 1040.
[25] K. Zhu, et al., Heteroatom-doped porous carbon nanoparticle-decorated carbon cloth (HPCN/CC) as efficient anode electrode for microbial fuel cells (MFCs), J. Clean. Prod. 336 (2022), 130374.
[26] Y. Liu, et al., Fundamental development and research of cathodic compartment in microbial fuel cells: a review, J. Environ. Chem. Eng. 10 (3) (2022), 107918.
[27] J. Chen, et al., Design and research progress of nano materials in cathode catalysts of microbial fuel cells: a review, Int. J. Hydrog. Energy 47 (41) (2022) 18098–18108.
[28] K. Zhao, et al., Bimetallic catalysts as electrocatalytic cathode materials for the oxygen reduction reaction in microbial fuel cell: a review, Green Energy Environ. 8 (4) (2022) 1043–1070.
[29] R. Moreno-Cervera, et al., Performance of a greywater cathode in a microbial fuel cell with three ion exchange membranes, J. Chem. Technol. Biotechnol. 94 (5) (2019) 1601–1612.
[30] J.X. Leong, et al., Ion exchange membranes as separators in microbial fuel cells for bioenergy conversion: a comprehensive review, Renew. Sust. Energ. Rev. 28 (Supplement C) (2013) 575–587.
[31] X. Zhang, et al., Separator characteristics for increasing performance of microbial fuel cells, Environ. Sci. Technol. 43 (21) (2009) 8456–8461.
[32] V. Baglio, et al., Proton exchange membranes based on the short-side-chain perfluorinated ionomer for high temperature direct methanol fuel cells, Desalination 199 (1–3) (2006) 271–273.
[33] J.R. Kim, et al., Power generation using different cation, anion, and ultrafiltration membranes in microbial fuel cells, Environ. Sci. Technol. 41 (3) (2007) 1004–1009.
[34] M. Rahimnejad, et al., Nafion as a nanoproton conductor in microbial fuel cells, Turk. J. Eng. Environ. Sci. 34 (4) (2011) 289–292.
[35] S.G. Flimban, et al., The effect of Nafion membrane fouling on the power generation of a microbial fuel cell, Int. J. Hydrog. Energy 45 (25) (2020) 13643–13651.
[36] I. Ieropoulos, J. Greenman, C. Melhuish, Improved energy output levels from small-scale microbial fuel cells, Bioelectrochemistry 78 (1) (2010) 44–50.
[37] D. Pant, et al., Use of novel permeable membrane and air cathodes in acetate microbial fuel cells, Electrochim. Acta 55 (26) (2010) 7710–7716.
[38] G. Papaharalabos, et al., A novel small scale microbial fuel cell design for increased electricity generation and waste water treatment, Int. J. Hydrog. Energy 40 (11) (2015) 4263–4268.
[39] Y. Zuo, S. Cheng, B.E. Logan, Ion exchange membrane cathodes for scalable microbial fuel cells, Environ. Sci. Technol. 42 (18) (2008) 6967–6972.
[40] W.-W. Li, et al., Recent advances in the separators for microbial fuel cells, Bioresour. Technol. 102 (1) (2011) 244–252.
[41] M. Shabani, et al., A critical review on recent proton exchange membranes applied in microbial fuel cells for renewable energy recovery, J. Clean. Prod. 264 (2020), 121446.
[42] S.S. Lim, et al., Sulfonated poly (ether ether ketone)/poly (ether sulfone) composite membranes as an alternative proton exchange membrane in microbial fuel cells, Int. J. Hydrog. Energy 37 (15) (2012) 11409–11424.
[43] V. Kugarajah, M. Sugumar, S. Dharmalingam, Nanocomposite membrane and microbial community analysis for improved performance in microbial fuel cell, Enzym. Microb. Technol. 140 (2020), 109606.
[44] S. Shahgaldi, et al., Performance enhancement of microbial fuel cell by PVDF/Nafion nanofibre composite proton exchange membrane, Fuel Process. Technol. 124 (2014) 290–295.
[45] V. Yousefi, et al., Effect of separator electrode assembly (SEA) design and mode of operation on the performance of continuous tubular microbial fuel cells (MFCs), Int. J. Hydrog. Energy 41 (1) (2016) 597–606.
[46] Y. Fan, H. Hu, H. Liu, Enhanced Coulombic efficiency and power density of air-cathode microbial fuel cells with an improved cell configuration, J. Power Sources 171 (2) (2007) 348–354.
[47] X. Zhang, et al., Scalable air cathode microbial fuel cells using glass fiber separators, plastic mesh supporters, and graphite fiber brush anodes, Bioresour. Technol. 102 (1) (2011) 372–375.
[48] B.R. Patel, et al., Durum wheat semolina-modified ceramic membranes as novel porous separators for enhanced power generation and wastewater remediation using microbial fuel cell, Bioresour. Technol. 361 (2022), 127752.
[49] B.R. Patel, M. Noroozifar, K. Kerman, Recent improvements of ceramic membranes in microbial fuel cells for bioelectricity generation and wastewater remediation: from fundamentals to scale-up applications, J. Environ. Chem. Eng. 10 (6) (2022), 108664.
[50] M. Cheraghipoor, et al., Production of greener energy in microbial fuel cell with ceramic separator fabricated using native soils: effect of lattice and porous SiO2, Fuel 284 (2021), 118938.
[51] V. Yousefi, D. Mohebbi-Kalhori, A. Samimi, Start-up investigation of the self-assembled chitosan/montmorillonite nanocomposite over the ceramic support as a low-cost membrane for microbial fuel cell application, Int. J. Hydrog. Energy 45 (7) (2020) 4804–4820.
[52] V. Yousefi, D. Mohebbi-Kalhori, A. Samimi, Equivalent electrical circuit modeling of ceramic-based microbial fuel cells using the electrochemical impedance spectroscopy (EIS) analysis, J. Renew. Energy Environ. 6 (1) (2019) 21–28.
[53] M. Cheraghipoor, et al., Comparative study of bioelectricity generation in a microbial fuel cell using ceramic membranes made of ceramic powder, Kalporgan's soil, and acid leached Kalporgan's soil, Energy 178 (2019) 368–377.
[54] V. Yousefi, D. Mohebbi-Kalhori, A. Samimi, Application of layer-by-layer assembled chitosan/montmorillonite nanocomposite as oxygen barrier film over the ceramic separator of the microbial fuel cell, Electrochim. Acta 283 (2018) 234–247.
[55] V. Yousefi, D. Mohebbi-Kalhori, A. Samimi, Ceramic-based microbial fuel cells (MFCs): a review, Int. J. Hydrog. Energy 42 (3) (2017) 1672–1690.
[56] V. Yousefi, Statistical investigation of pivotal physical and chemical factors on the performance of ceramic-based microbial fuel cells, Energy Harvesting Syst. 9 (2) (2022) 239–252.
[57] S. Kondaveeti, et al., Low-cost separators for enhanced power production and field application of microbial fuel cells (MFCs), Electrochim. Acta 132 (2014) 434–440.

[58] K. Senthilkumar, et al., Chapter 2 - A review on scaling-up of microbial fuel cell: challenges and opportunities, in: D.A. Jadhav, et al. (Eds.), Scaling Up of Microbial Electrochemical Systems, Elsevier, 2022, pp. 13–28.
[59] R. Selvasembian, et al., Recent progress in microbial fuel cells for industrial effluent treatment and energy generation: fundamentals to scale-up application and challenges, Bioresour. Technol. 346 (2022), 126462.
[60] S. Yang, et al., Development of miniature self-powered single-chamber microbial fuel cell and its response mechanism to copper ions in high and trace concentration, Sci. Total Environ. 834 (2022), 155367.
[61] M.H. Do, et al., Microbial fuel cell-based biosensor for online monitoring wastewater quality: a critical review, Sci. Total Environ. 712 (2020), 135612.
[62] H. Kaneshiro, et al., A milliliter-scale yeast-based fuel cell with high performance, Biochem. Eng. J. 83 (2014) 90–96.
[63] F. Qian, D.E. Morse, Miniaturizing microbial fuel cells, Trends Biotechnol. 29 (2) (2011) 62–69.
[64] S. Choi, Microscale microbial fuel cells: advances and challenges, Biosens. Bioelectron. 69 (2015) 8–25.
[65] S. Mateo, et al., On the staking of miniaturized air-breathing microbial fuel cells, Appl. Energy 232 (2018) 1–8.
[66] I.A. Ieropoulos, J. Greenman, C. Melhuish, Miniature microbial fuel cells and stacks for urine utilisation, Int. J. Hydrog. Energy 38 (1) (2013) 492–496.
[67] Y. Fan, et al., Miniature microbial fuel cells integrated with triggered power management systems to power wastewater sensors in an uninterrupted mode, Appl. Energy 302 (2021), 117556.
[68] B.R. Ringeisen, et al., High power density from a miniature microbial fuel cell using Shewanella oneidensis DSP10, Environ. Sci. Technol. 40 (8) (2006) 2629–2634.
[69] H. Richter, et al., Electricity generation by Geobacter sulfurreducens attached to gold electrodes, Langmuir 24 (8) (2008) 4376–4379.
[70] M. Quaglio, et al., A fluid dynamics perspective on material selection in microbial fuel cell-based biosensors, Int. J. Hydrog. Energy 44 (9) (2019) 4533–4542.
[71] I. Ieropoulos, J. Greenman, C. Melhuish, Microbial fuel cells based on carbon veil electrodes: stack configuration and scalability, Int. J. Energy Res. 32 (13) (2008) 1228–1240.
[72] S.P. Jung, S. Son, B. Koo, Reproducible polarization test methods and fair evaluation of polarization data by using interconversion factors in a single chamber cubic microbial fuel cell with a brush anode, J. Clean. Prod. 390 (2023), 136157.
[73] I. Chakraborty, et al., Novel low cost proton exchange membrane made from sulphonated biochar for application in microbial fuel cells, Mater. Chem. Phys. 239 (2020), 122025.
[74] B. Padha, et al., Electrochemical impedance spectroscopy (EIS) performance analysis and challenges in fuel cell applications, J. Electrochem. Sci. Technol 13 (2) (2022) 167–176.
[75] H. Wang, et al., Electrochemical impedance spectroscopy applied to microbial fuel cells: a review, Front. Microbiol. 13 (2022).
[76] S. Elakkiya, et al., Enhancement of fuel cell properties in polyethersulfone and sulfonated poly (ether ether ketone) membranes using metal oxide nanoparticles for proton exchange membrane fuel cell, Int. J. Hydrog. Energy 43 (47) (2018) 21750–21759.
[77] S.N. Kardi, et al., Investigating effect of proton-exchange membrane on new air-cathode single-chamber microbial fuel cell configuration for bioenergy recovery from Azorubine dye degradation, Environ. Sci. Pollut. Res. 26 (21) (2019) 21201–21215.
[78] K.J. Chae, et al., Mass transport through a proton exchange membrane (nafion) in microbial fuel cells, Energy Fuel 22 (1) (2008) 169–176.
[79] B. Hou, J. Sun, Y.-y. Hu, Simultaneous Congo red decolorization and electricity generation in air-cathode single-chamber microbial fuel cell with different microfiltration, ultrafiltration and proton exchange membranes, Bioresour. Technol. 102 (6) (2011) 4433–4438.
[80] E. Yang, K.-J. Chae, I.S. Kim, Assessment of different ceramic filtration membranes as a separator in microbial fuel cells, Desalin. Water Treat. 57 (58) (2016) 28077–28085.
[81] F. Zhao, R.C.T. Slade, J.R. Varcoe, Techniques for the study and development of microbial fuel cells: an electrochemical perspective, Chem. Soc. Rev. 38 (7) (2009) 1926–1939.
[82] G. Palanisamy, S. Thangarasu, T.H. Oh, Effect of sulfonated inorganic additives incorporated hybrid composite polymer membranes on enhancing the performance of microbial fuel cells, Polymers 15 (5) (2023) 1294.
[83] G.J. Brug, et al., The analysis of electrode impedances complicated by the presence of a constant phase element, J. Electroanal. Chem. Interfacial Electrochem. 176 (1) (1984) 275–295.
[84] Y. Fang, et al., Layer-by-layer construction of in situ formed polypyrrole and bacterial cells as capacitive bioanodes for paper-based microbial fuel cells, J. Mater. Chem. A 10 (9) (2022) 4915–4925.
[85] H.-B. Khalili, D. Mohebbi-Kalhori, M.S. Afarani, Microbial fuel cell (MFC) using commercially available unglazed ceramic wares: low-cost ceramic separators suitable for scale-up, Int. J. Hydrog. Energy 42 (12) (2017) 8233–8241.
[86] G. Hernández-Flores, et al., Characteristics of a single chamber microbial fuel cell equipped with a low cost membrane, Int. J. Hydrog. Energy 40 (48) (2015) 17380–17387.
[87] M. Ghasemi, et al., Sulfonated poly ether ether ketone with different degree of sulphonation in microbial fuel cell: application study and economical analysis, Int. J. Hydrog. Energy 41 (8) (2016) 4862–4871.
[88] B. Tiwari, M.T. Noori, M. Ghangrekar, A novel low cost polyvinyl alcohol-Nafion-borosilicate membrane separator for microbial fuel cell, Mater. Chem. Phys. 182 (2016) 86–93.
[89] J. Moon, S. Kondaveeti, B. Min, Evaluation of low-cost separators for increased power generation in single chamber microbial fuel cells with membrane electrode assembly, Fuel Cells 15 (1) (2015) 230–238.